JOURNAL OF GUIDANCE, CONTROL, AND DYNAMICS
Vol. 29, No. 6, November–December 2006

Indirect Optimization of Spiral Trajectories

Christopher L. Ranieri* and Cesar A. Ocampo†
University of Texas at Austin, Austin, Texas 78712

DOI: 10.2514/1.19539

Indirect optimization is used to compute minimum propellant spiral escapes and captures. A two-step estimation process generates accurate estimates of the Lagrange multipliers. The first step, an adjoint control transformation, converts the thrust unit direction vector to the actual multipliers that control the trajectory. Next, curve fits are matched with the values of the initial multipliers from spirals found with the adjoint control transformation and used to extrapolate the multipliers for longer spirals. Spherical rather than Cartesian coordinates are used because the spherical multipliers evolve in a well-behaved fashion, allowing the accurate extrapolation of the multipliers. Long-duration Earth escapes are presented for spirals as long as 150 days. Solutions are also presented with control limits on the thrust or specific impulse. Additionally, a transformation is developed that converts the spherical multipliers to the corresponding Cartesian multipliers and vice versa. Another transformation is developed to convert the optimal multipliers for two-dimensional, planar equatorial spirals into the optimal multipliers for planar-inclined orbits in either Cartesian or spherical coordinates in which the initial orbit may have arbitrary values for inclination, right ascension of the ascending node, and argument of periapsis.

Nomenclature

A–F	=	temporary variables used in transformation between two and three dimensions
A_1	=	coefficient for estimation of costates
a	=	thrust acceleration magnitude
B_1	=	exponent for estimation of costates
$\boldsymbol{c}$	=	targeted constraint vector for boundary value problem
$\boldsymbol{e}$	=	unit vector for coordinate frames
f	=	true anomaly
G	=	Bolza function
H	=	Hamiltonian
$\boldsymbol{h}$	=	angular momentum vector
i	=	inclination
J	=	cost function
m	=	spacecraft mass
P	=	spacecraft power
r, θ, Φ	=	spherical position components
t	=	time
$\boldsymbol{u}$	=	thrust acceleration unit direction vector
V_*	=	velocity component in * direction
$\boldsymbol{x}$	=	spacecraft state vector
x, y, z	=	Cartesian position components
$\boldsymbol{z}$	=	parameter vector for boundary value problem
α	=	in-plane thrust angle used in adjoint control transformation
β	=	true anomaly plus argument of perigee
γ	=	out-of-plane thrust angle used in adjoint control transformation
ε	=	spacecraft energy
λ	=	costates
μ	=	gravitational parameter
ρ	=	multiplier associated with targeted conditions
ω	=	argument of perigee
Ω	=	right ascension of ascending node
*	=	terms in matrices that do not affect the final solution

Subscripts

f	=	condition at time t_f
tar	=	target
0	=	condition at time t_0

Presented as Paper AAS 05-372 at the AAS/AIAA Astrodynamics Specialists Conference, South Lake Tahoe, CA, 7–11 August 2005; received 17 August 2005; revision received 5 April 2006; accepted for publication 18 April 2006.

*National Defense Science and Engineering Graduate Research Fellow and Graduate Student, Department of Aerospace Engineering and Engineering Mechanics, 1 University Station, Mail Stop C0600; cxr288@mail.utexas.edu.

†Associate Professor, Department of Aerospace Engineering and Engineering Mechanics, 1 University Station C0600; cesar.ocampo@mail.utexas.edu.

Introduction

AN indirect optimization procedure is presented for optimizing spiral trajectories and two estimation techniques are developed and used in conjunction to determine accurate initial guesses for the unknown Lagrange multipliers or costates that govern the behavior of the spacecraft trajectory. Understanding the dynamics and optimization of spiral trajectories is an important cornerstone for constructing missions such as a low Earth orbit (LEO) to low Mars orbit (LMO) transfer. For such a problem, the overall trajectory can be categorized by three separate phases: Earth escape spiral, heliocentric transfer leg, and Mars capture spiral. Analysis and derivation of the appropriate optimality conditions for the heliocentric legs, particularly for time-constrained, round-trip missions, has previously been developed [1,2]. The goal of this work is to obtain a better understanding of the dynamics of the most complicated portion of the transfers, the spirals, and use these findings in future work to find LEO-to-LMO missions with the fewest simplifying assumptions. Although there is a large body of research on optimizing spirals with direct methods, analytical methods, and other approximate solutions, the research presented here focuses on indirect optimization. Other works have analyzed end-to-end LEO-to-LMO [3,4] or low lunar orbit (LLO) [5–8] missions but often simplify the engine dynamics or use a different cost function than used here for the spirals. Other works [9,10] have attempted to develop techniques to accurately estimate the costates for continuously burning engines but analyze minimum time rather than minimum fuel missions and only consider constant thrust cases.

For a given engine performance, the aim of a typical spacecraft trajectory optimization problem is to minimize the fuel. The engine model used is a variable specific impulse (VSI) engine in which the power is constant but the thrust acceleration magnitude can be throttled accordingly. A generalized cost function is used that allows the fuel usage to be determined based on the user-supplied values of the initial mass and vehicle power. Past research, in which the spirals

use constant thrust or nearly constant thrust for almost the entirety of the spiral, instead of directly minimizing the fuel, attempt to maximize the energy with respect to the spiral planet [3–7]. Other works do use VSI engines for the spirals and minimize fuel usage but the spirals presented are for short-duration spirals of less than five days [8], whereas this research finds fuel-optimal spirals with much longer times of flight. The indirect optimization problem is solved as an optimal control problem; the associated Euler–Lagrange equations are integrated numerically. A boundary value problem is formulated in terms of the costates and solved to optimize the trajectory. From this formulation, the values of the thrust acceleration magnitude and direction are determined to be continuous functions of the costates.

In general, the targeted state condition at the final time is a user-specified value of the energy relative to the spiral planet. For the escapes, the spiral planet is Earth and the targeted energy value is zero. Capture spirals at Mars are also explored. The equations of motion and costate equations are developed in both Cartesian and spherical coordinates. Spherical coordinates are found to be the better choice for generating spirals. Other works [3–8] have used spherical coordinates for spirals, but this work analyzes the specific benefits of these coordinates. In particular, the relationship between the behaviors of the costates vs the time of flight (TOF) provides insight to the dynamics of the spirals in the spherical frame.

In Cartesian space, half of the costates exhibit no discernible trend as the TOF is increased. However, in polar coordinates, three of the four unknown initial costates are very well-behaved. This allows curves to be accurately fitted to the values of the initial costates. Converged shorter duration spirals are fairly easy to find, especially when using the adjoint control transformation (ACT). The ACT allows estimates of the costates to be made intelligently by converting the acceleration unit direction vector expressed in spherical angles to the actual costates that control the trajectory. This method, although shown previously [1] for Cartesian coordinates, is now developed for spherical coordinates. The costates from these shorter spirals form the first data sets that are used to form the curve fits. The curves can then be used to extrapolate the unknown initial costates for a spiral with a different TOF. An estimate of the fourth costate can be formed by estimating the initial acceleration magnitude in the same manner and then analyzing a few algebraic relationships.

This costate estimation method allows the user to easily find optimal spirals with longer times of flight. Traditionally, even with polar coordinates, it is very difficult to generate optimal spirals without making simplifying assumptions about the dynamics of the system (e.g. constant, fixed thrust). The capability to accurately form an initial estimate for the unknowns is vital when analyzing longer spirals. Solutions are presented with spiral times as long as 150 days, which includes over 560 revolutions around the Earth. Because of the high number of revolutions, the integration is slow as it incorporates a large number of steps to accurately reflect the trajectory, making an accurate initial estimate even more vital to quickly solving such missions. Using the curves to estimate the costates generates an accurate guess that converges quickly.

Solutions are also explored where the thrust acceleration is constrained along the velocity vector and constraints are placed on the engine performance. Although the equations are not presented in detail here for these solutions, the penalty to the cost function for constraining the thrust along the velocity vector is not very significant but it does increase the cost a measurable amount [11]. Three-dimensional solutions are also examined. The eventual goal is to link the spirals to heliocentric legs, allowing the full indirect optimization of a LEO–LMO mission.

Spherical Equations of Motion

A spherical coordinate system is used with two angles and the position magnitude. The inertial Cartesian and spherical frames are related by the following rotation.

$$\begin{bmatrix} e_r \\ e_\theta \\ e_\phi \end{bmatrix} = \begin{bmatrix} \cos\phi\cos\theta & \cos\phi\sin\theta & \sin\phi \\ -\sin\theta & \cos\theta & 0 \\ -\sin\phi\cos\theta & -\sin\phi\sin\theta & \cos\phi \end{bmatrix} \begin{bmatrix} e_x \\ e_y \\ e_z \end{bmatrix} \tag{1}$$

The state and its derivative are defined as follows:

$$\boldsymbol{x} = \begin{bmatrix} r \\ \theta \\ \phi \\ v_r \\ v_\theta \\ v_\phi \end{bmatrix} \tag{2}$$

$$\dot{\boldsymbol{x}} = \begin{bmatrix} v_r \\ v_\theta/r\cos\phi \\ v_\phi/r \\ \left(v_\theta^2 + v_\phi^2\right)/r - \mu/r^2 + au_r \\ v_\theta(v_\phi\tan\phi - v_r)/r + au_\theta \\ -\left(v_r v_\phi + v_\theta^2\tan\phi\right)/r + au_\phi \end{bmatrix} \tag{3}$$

To minimize the spacecraft propellant for a VSI engine, the spacecraft mass and power are decoupled from the problem and the minimum fuel problem can be based solely on the accumulated thrust acceleration [12].

$$\frac{1}{m_f} - \frac{1}{m_0} = \frac{1}{2}\int_{t0}^{tf} (a^2/P)\,\mathrm{d}t \tag{4}$$

The optimal value for the power for an unconstrained VSI engine is the maximum power level and can be removed from this equation. From this cost function, using optimal control theory, a boundary value problem is formed that, when satisfied, meets all of the first-order conditions for optimality [13].

$$J = \min\left[\frac{1}{2}\int_{t0}^{tf} a^2\,\mathrm{d}t\right] = -\frac{1}{2}\int_{t0}^{tf} a^2\,\mathrm{d}t \tag{5}$$

The Hamiltonian and the associated optimal controls are

$$H = \boldsymbol{\lambda}^T\dot{\boldsymbol{x}} - a^2/2 \tag{6}$$

$$u_r^2 + u_\theta^2 + u_\phi^2 = 1 \tag{7}$$

$$\boldsymbol{u} = \boldsymbol{\lambda}_{\mathbf{v}}/\lambda_v \tag{8}$$

$$a = \lambda_v \tag{9}$$

Once the boundary value problem has been solved to optimize the cost function laid out in Eq. (5), the general kinematics problem can be converted to a specific mission scenario by solving for the final mass m_f in Eq. (4) by specifying values for the vehicle power and initial mass value.

$$m_f = m_0 P_{\max}/\left(P_{\max} + m_0^* J\right) \tag{10}$$

Next, using the definition of the Hamiltonian, costate equations can be found.

$$\dot{\boldsymbol{\lambda}} = -H_{\mathbf{x}}^T \tag{11}$$

$$\begin{bmatrix} \dot{\lambda}_r \\ \dot{\lambda}_\theta \\ \dot{\lambda}_\phi \\ \dot{\lambda}_{vr} \\ \dot{\lambda}_{v\theta} \\ \dot{\lambda}_{v\phi} \end{bmatrix} = \begin{bmatrix} (\lambda_\theta v_\theta + \lambda_\phi v_\phi \cos\phi)/(r^2\cos\phi) + \lambda_{vr}\left[\left(v_\theta^2 + v_\phi^2\right)/r^2 - 2\mu/r^3\right] + \\ \lambda_{v\theta}(v_\theta v_\phi \tan\phi - v_r v_\theta)/r^2 - \lambda_{v\phi}\left(v_r v_\phi + v_\theta^2 \tan\phi\right)/r^2 \\ 0 \\ \left(\lambda_{v\phi} v_\theta^2 - \lambda_{v\theta} v_\theta v_\phi\right)\sec^2\phi/r - \lambda_\theta v_\theta \tan\phi/(r\cos\phi) \\ -\lambda_r + (\lambda_{v\theta} v_\theta + \lambda_{v\phi} v_\phi)/r \\ [\lambda_{v\theta}(v_r - v_\phi \tan\phi) + 2\lambda_{v\phi} v_\theta \tan\phi - \lambda_\theta/\cos\phi - 2\lambda_{vr} v_\theta]/r \\ (\lambda_{v\phi} v_r - \lambda_\phi - 2\lambda_{vr} v_\phi - \lambda_{v\theta} v_\theta \tan\phi)/r \end{bmatrix} \tag{12}$$

The equivalent costate equations in Cartesian coordinates have been derived previously [1]:

$$\begin{bmatrix} \dot{\lambda}_x \\ \dot{\lambda}_y \\ \dot{\lambda}_z \\ \dot{\lambda}_{vx} \\ \dot{\lambda}_{vy} \\ \dot{\lambda}_{vz} \end{bmatrix} = \begin{bmatrix} \mu[\lambda_{vx}(r^2 - 3x^2) - 3xy\lambda_{vy} - 3xz\lambda_{vz}]/r^5 \\ \mu[-3xy\lambda_{vx} + \lambda_{vy}(r^2 - 3y^2) - 3yz\lambda_{vz}]/r^5 \\ \mu[-3xz\lambda_{vx} - 3yz\lambda_{vy} + \lambda_{vz}(r^2 - 3z^2)]/r^5 \\ -\lambda_x \\ -\lambda_y \\ -\lambda_z \end{bmatrix} \tag{13}$$

The spirals have a fixed transfer time to a targeted energy relative to the spiral planet. This constraint is adjoined to the Bolza function.

$$\varepsilon = v^2/2 - \mu/r \tag{14}$$

$$G = \rho_{\varepsilon f}(\varepsilon_f - \varepsilon_{\text{tar}}) \tag{15}$$

The Bolza function is adjoined to the cost function to form the modified cost function, J'.

$$J' = G - \frac{1}{2}\int_{t0}^{tf} a^2 \, \mathrm{d}t \tag{16}$$

As the boundary value problem is derived, the appropriate conditions in both Cartesian and spherical coordinates are shown.

$$\mathbf{G}_{\mathbf{xf}}^{T} = \boldsymbol{\lambda}_{\mathbf{f}} = \begin{bmatrix} \mu v_f x_f r^{-3} \\ \mu v_f y_f r^{-3} \\ \mu v_f z_f r^{-3} \\ \rho_f v_{xf} \\ \rho_f v_{yf} \\ \rho_f v_{zf} \end{bmatrix}_{6x1}^{xyz} = \begin{bmatrix} v_{\varepsilon f}\mu/r^2 \\ 0 \\ 0 \\ \rho_{\varepsilon f} v_{rf} \\ \rho_{\varepsilon f} v_{\theta f} \\ \rho_{\varepsilon f} v_{\phi f} \end{bmatrix}_{6x1}^{r\theta\phi} \tag{17}$$

Because $\lambda_{\theta f}$ is equal to zero and λ_θ is a constant, it can be eliminated from the unknowns. The remaining unknowns and corresponding targeted conditions at t_f are

$$\boldsymbol{z} = \begin{bmatrix} \lambda_{x0} \\ \lambda_{y0} \\ \lambda_{z0} \\ \lambda_{vx0} \\ \lambda_{vy0} \\ \lambda_{vz0} \\ v_{\varepsilon f} \end{bmatrix}_{7x1}^{xyz} = \begin{bmatrix} \lambda_{r0} \\ \lambda_{\phi 0} \\ \lambda_{vr0} \\ \lambda_{v\theta 0} \\ \lambda_{v\phi 0} \\ v_{\varepsilon f} \end{bmatrix}_{6x1}^{r\theta\phi} \tag{18}$$

$$\boldsymbol{c} = \begin{bmatrix} \varepsilon_f - \varepsilon_{\text{tar}} \\ \left(\mathbf{G}_{\mathbf{xf}} - \boldsymbol{\lambda}_{\mathbf{f}}^{\mathbf{T}}\right)_{6x1} \end{bmatrix}_{7x1}^{xyz} = \begin{bmatrix} \varepsilon_f - \varepsilon_{\text{tar}} \\ \lambda_{rf} - \rho_{\varepsilon f}\mu/r^2 \\ \lambda_{\phi f} \\ (\boldsymbol{\lambda}_{\text{vf}} - \rho_{\varepsilon f}\mathbf{v}_{\mathbf{f}})_{3x1} \end{bmatrix}_{6x1}^{r\theta\phi} = 0 \tag{19}$$

In many cases, it is easier to examine just a two-dimensional polar case, reducing the system to four polar unknowns or five Cartesian unknowns.

Adjoint Control Transformation

The initial estimates of the unknown vector can be given more physical meaning with the use of an adjoint control transformation (ACT). The velocity costates can be replaced by spherical angles that describe the direction of the thrust [7,14] These values can then be used to solve for the actual costate vector. This transformation is achieved by first expressing the thrust direction vector as spherical angles in a vehicle-centered coordinate frame.

$$\boldsymbol{u} = \begin{bmatrix} u_r \\ u_\theta \\ u_\varphi \end{bmatrix} = \begin{bmatrix} \cos\alpha\cos\gamma \\ \sin\alpha\cos\gamma \\ \sin\gamma \end{bmatrix} \tag{20}$$

Its derivative, which is used in transforming to the actual costates, is:

$$\dot{\boldsymbol{u}} = \begin{bmatrix} \dot{u}_r \\ \dot{u}_\theta \\ \dot{u}_\varphi \end{bmatrix} = \begin{bmatrix} -\dot{\alpha}\sin\alpha\cos\gamma - \dot{\gamma}\cos\alpha\sin\gamma \\ \dot{\alpha}\cos\alpha\cos\gamma - \dot{\gamma}\sin\alpha\sin\gamma \\ \dot{\gamma}\cos\gamma \end{bmatrix} \tag{21}$$

Equation (8) can be rewritten to solve for the velocity costate vector and its time derivatives solely as functions of the spherical thrust angles, their time rates of change, and the magnitude of the velocity costate by inserting Eqs. (20) and (21) into Eqs. (22) and (23).

$$\boldsymbol{\lambda}_{\mathbf{V}} = \lambda_v \mathbf{u} \tag{22}$$

$$\dot{\boldsymbol{\lambda}}_{\mathbf{v}} = \dot{\lambda}_v \mathbf{u} + \lambda_v \dot{\mathbf{u}} \tag{23}$$

Substituting Eq. (12) into (23) and rearranging, the following equations can be found:

$$\dot{\lambda}_v = [\lambda_{v\theta}(v_r - v_\phi \tan\phi)/r + 2\lambda_{v\phi} v_\theta \tan\phi/r - 2\lambda_{vr} v_\theta/r - \lambda_\theta/r\cos\phi - \lambda_v \dot{u}_\theta]/u_\theta \tag{24}$$

$$\lambda_r = (\lambda_{v\theta} v_\theta + \lambda_{v\phi} v_\phi)/r - \lambda_v \dot{u}_r - \dot{\lambda}_v u_r \tag{25}$$

$$\lambda_\phi = \lambda_{v\phi} v_r - \lambda_{v\theta} v_\theta \tan\phi - 2\lambda_{vr} v_\phi - (\dot{\lambda}_v u_\varphi + \lambda_v \dot{u}_\varphi) r \tag{26}$$

Using Eqs. (20–22) and (24–26), the unknown costates can be found in terms of the spherical thrust angles, their time rates of change, and the magnitude of the velocity costate. Symbolically, the ACT is described as:

$$\begin{bmatrix} \alpha \\ \beta \\ \dot{\alpha} \\ \dot{\beta} \\ \lambda_v \\ \lambda_\theta \end{bmatrix} \rightarrow \text{ACT} \rightarrow \begin{bmatrix} \lambda_r \\ \lambda_\theta \\ \lambda_\phi \\ \lambda_{vr} \\ \lambda_{v\theta} \\ \lambda_{v\phi} \end{bmatrix} \tag{27}$$

In most cases, the ACT can be reduced in size by one by removing λ_θ, which is a known constant of zero for all problems analyzed here.

Costate Transformations (Polar to Cartesian and Vice Versa)

The optimal value of the costates found in the polar case can be transformed into the costates in the Cartesian frame or vice versa. In either frame, the initial acceleration magnitude, which is also the velocity costate magnitude, and its direction are identical. From the definition of the thrust direction in Eq. (8) and rotating from the polar to Cartesian frame, equations are found that relate the velocity costate components in the polar plane to the velocity costate components in the Cartesian frame in terms of the polar velocity costates and the polar angle θ.

$$\begin{bmatrix} \lambda_{vx} \\ \lambda_{vy} \end{bmatrix} = \lambda_v \begin{bmatrix} u_x \\ u_y \end{bmatrix} = \begin{bmatrix} \lambda_{vr}\cos\theta - \lambda_{v\theta}\sin\theta \\ \lambda_{vr}\sin\theta + \lambda_{v\theta}\cos\theta \end{bmatrix} \tag{28}$$

Next, the time derivative of both sides of Eq. (28) is taken. Inserting the appropriate terms from Eqs. (3), (12), and (13) into the time derivative of Eq. (28) yields the position costate in Cartesian space written in terms of the polar costates and the polar angle θ.

$$\begin{bmatrix} \lambda_x \\ \lambda_y \end{bmatrix} = \begin{bmatrix} \lambda_r\cos\theta + (\lambda_{v\theta}v_r - \lambda_\theta - \lambda_{vr}v_\theta)\sin\theta/r \\ \lambda_r\sin\theta + (\lambda_\theta + \lambda_{vr}v_\theta - \lambda_{v\theta}v_r)\cos\theta/r \end{bmatrix} \tag{29}$$

Using the same logic, the polar costates can be recovered from the Cartesian costates.

$$\begin{bmatrix} \lambda_r \\ \lambda_\theta \\ \lambda_{vr} \\ \lambda_{v\theta} \end{bmatrix} = \begin{bmatrix} \lambda_x\cos\theta + \lambda_y\sin\theta \\ v_r(\lambda_{vy}x - \lambda_{vx}y)/r - v_\theta(\lambda_{vx}x + \lambda_{vy}y)/r + \lambda_y x - \lambda_x y \\ \lambda_{vx}\cos\theta + \lambda_{vy}\sin\theta \\ -\lambda_{vy}\sin\theta + \lambda_{vy}\cos\theta \end{bmatrix} \tag{30}$$

Estimating the Costates

For all trajectories presented, a variable step size, fifth-order Cash–Karp Runga–Kutta method is used [15]. The boundary value problems are solved with a nonlinear equation solver that uses a modified Newton's method coupled with Broyden's method for improving the Jacobian [16]. In spherical coordinates, a process is developed to accurately estimate the costates. The first step involves finding the optimal initial costates for spirals with short times of flight (0–5 days) using the ACT. Plotting the optimal initial values for λ_r, $\lambda_{v\theta}$, ρ_f, and $a_0(=\lambda_{v0})$ vs the TOF shows that they closely follow power law curves. Using the curve fits from the first 5 days worth of data points generates accurate estimates of the costates for times of flight of approximately 15–20 days. The fourth costate, λ_{vr}, cannot be estimated using the curve fits but an estimate of its magnitude can still be determined. First, an estimate of $\lambda_{v\theta 0}$ and a_0 are made using the curve fits. Using Eq. (9), the magnitude of the initial optimal λ_{vr} can be estimated.

$$|\lambda_{vr0}| = \left(a_0^2 - \lambda_{v\theta 0}^2\right)^{1/2} \tag{31}$$

The curve fits are then recalibrated to incorporate the new converged data points up to 15–20 days and the updated curve fits are then accurate out to 40–60 days and possibly much longer, depending on the particular problem (150 days is the maximum tested). This process provides accurate estimates of all the unknowns. It is highly unlikely that the solution will converge when attempting to find the optimal costates for longer spirals with random guesses. The region of convergence for a slight deviation from the curve fits is not directly quantified as it depends on how large a time extrapolation is being used, the number of data points used to form each curve fit, and the root-solving algorithm used. If convergence troubles are encountered, recalculate the curve fits using all the available data and/or reduce the extrapolation of the time to a smaller step from the set of already-converged data points.

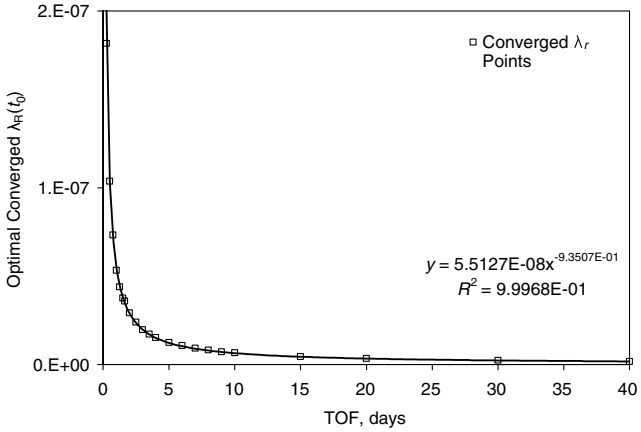

Fig. 1 Optimal initial λ_r vs TOF and curve fit.

Figure 1 is an example with the curve fits generated using Microsoft Excel's Trendline option where the accuracy of the curve fit is described by the value for R^2. The closer its value is to unity, the closer the curve fit is to an exact match of the data. Because the curves are found for the costates based on the cost function of Eq. (5), these estimation equations can be used for VSI trajectories with any initial mass and vehicle power. The curves are generated for an escape from an initial circular orbit in the equatorial plane and a semimajor axis of 7500 km. Other initial orbits can be chosen and although the four curve fits will take similar shapes, the specific estimation equations will be different. Additionally, the process can also estimate the costates for capture spirals. For capture spirals, the unknown costates are actually the final costates at the point of insertion into the target orbit around Mars as the solution is integrated backwards in time to a target of zero energy with respect to Mars. Capture spirals to a 4500 km circular orbit up to 70 days long are found in this manner.

The four curve fit equations and their accuracy R^2 are shown in Table 1. The estimates are based on Eq. (32) where the units of t are days and the units of A_1 are determined by dimensional analysis to match whatever parameter is being estimated. However, they really have no direct physical significance, as A_1 is just the empirical data fitting coefficient.

$$\text{Estimate} = A_1 t^{-B_1} \tag{32}$$

In contrast, the corresponding costates in Cartesian space do not behave regularly, particularly for flight times of 0–10 days. Using the transformations defined by Eqs. (28) and (29), the optimal Cartesian costates are found from the converged polar costates. The solutions are verified by checking that the Cartesian optimality targets are satisfied. The transformation allows the full range of flight times to be run in Cartesian space from the polar solutions, showing that the Cartesian curves do dampen for longer flight times but the earlier irregularities prohibit curve fits being generated initially, hence the choice of spherical coordinates.

Table 1 Estimation coefficients for spiral escape from $a = 7500$ km and $e = 0$.

TOF, days	λ_r: A_1	λ_r: B_1	$\lambda_{v\theta}$: A_1	$\lambda_{v\theta}$: B_1	ρ_f: A_1	ρ_f: B_1	a_0: A_1	a_0: B_1
$0-150+$	$5.5127E-08$	$9.3507E-01$	$5.6558E-05$	$9.3271E-01$	$1.5676E-05$	$7.0429E-01$	$5.6721E-05$	$9.3336E-01$
	λ_r Curve fit	$R^2 = 9.9968E-01$	$\lambda_{v\theta}$ Curve fit	$R^2 = 9.9968E-01$	ρ_f Curve fit	$R^2 = 9.9968E-01$	a_0 Curve fit	$R^2 = 9.9968E-01$

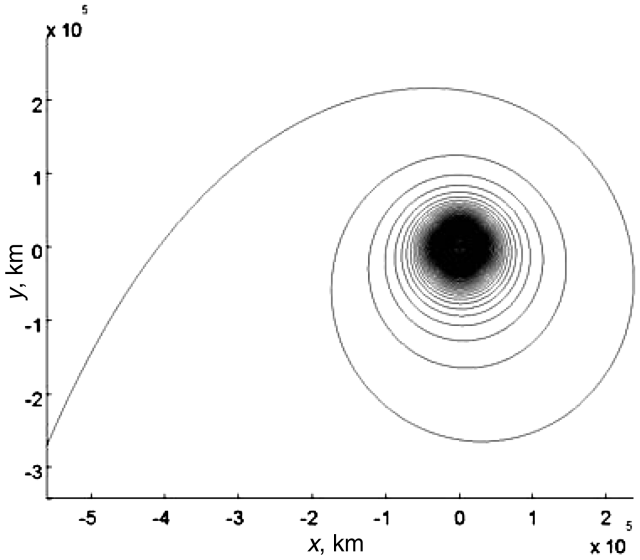

Fig. 2 Earth spiral escape: 150_days, 560 revolutions.

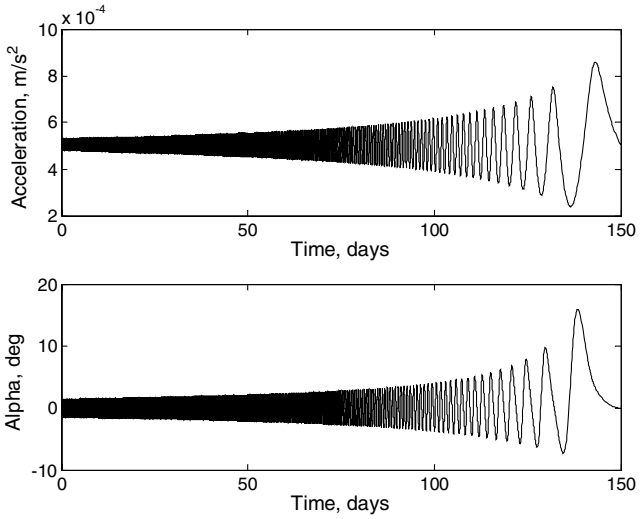

Fig. 3 Acceleration and angle between thrust and velocity vectors vs time.

Using Eq. (32) and Table 1, the costates for a 150-day spiral were estimated. This estimate easily converged to the optimal solution shown in Fig. 2 and encompasses almost 560 revolutions before escaping. The acceleration magnitude and angle between the thrust and the velocity vectors are shown in Fig. 3. From Eqs. (8) and (17), the thrust and velocity vectors must be collinear for an optimal solution [5] at the final time, which is shown in Fig. 3.

Converting the Cost Function to Allow I_{sp} and Thrust Constraints

The cost function in Eq. (5) cannot consider constraints on the engine parameters such as the achievable range of I_{sp}. Therefore, the formulation of Eq. (5) may only be useful as a first step in mission planning. To include these limits, the cost function that directly maximizes final mass and considers the mass as a state and the power as a control must be used.

$$J = \max(m_f) \tag{33}$$

The costates associated with the cost function laid out in Eq. (5) can be converted to the costates linked to Eq. (33). A scalar, (m^2/P), can be multiplied to the costates found using Eq. (5), to find the costates that satisfy the boundary value problem derived from Eq. (33).

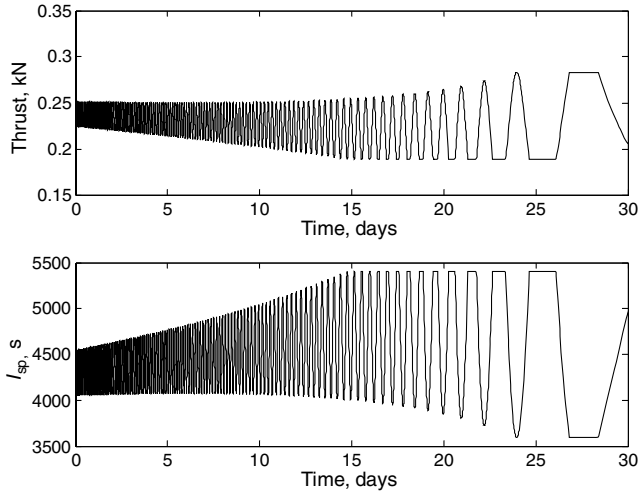

Fig. 4 Day escape, thrust, and I_{sp} vs time; $I_{sp} = 3600$–5400 s, 30-day escape.

Multiplying the cost function of Eq. (5) by m^2/P and using Eq. (35) and the mass flow rate T/c, it can be shown that the new cost function is Eq. (36).

$$J' = (m^2/P)J = -\frac{1}{2}\int_{t0}^{tf} (m^2 a^2/P)\,\mathrm{d}t \tag{34}$$

$$T = ma = 2P/c \tag{35}$$

$$J' = -\int_{t0}^{tf} |\dot{m}|\,\mathrm{d}t = -m_{\mathrm{prop}} \tag{36}$$

The result of maximizing Eq. (36) is identical to Eq. (33) and multiplying the initial costates of Eq. (5) by $m_0^2/P_{\max}$ yields the initial costates that satisfy the boundary value problem of Eq. (33). A converged solution for a specific vehicle mass and power and an unconstrained engine is found using this scalar factor and forms the first guess for missions with bounds on either I_{sp} or thrust. Then, increasingly more stringent engine constraints are imposed until the constraints are at their desired levels. Using the cost function in Eq. (33), adding the mass to the state, and imposing the control limits does affect the costate equations and the controls [1,2]. The transformation is useful when examining different legs of a mission, with the LEO–LMO mission as an example. Constraints may vary for different parts of the mission, such as constrained thrust during escape but variable thrust during heliocentric portions. In this case, it is beneficial to use the general cost function that can be scaled to any vehicle during the heliocentric legs and scale the results to match the specific mission constraint that may be imposed and active during the spirals. For the spiral escape example presented, the vehicle weighs 100,000 kg and has a power of 5 MW. The initial orbit is circular at 7500 km and has no inclination. Figure 4 shows the control history for thrust and I_{sp} when I_{sp} constraints are imposed.

Two-Dimensional to Three-Dimensional Spirals

A transformation is developed that takes an optimized two-dimensional spiral and rotates the solution into three dimensions. The transformation is useful when examining problems where the coordinate frame choice must be fixed by other problem considerations, such as being aligned with the Earth's ecliptic plane, and yet initial orbits at Earth may be desired that are inclined with respect to the chosen frame. This transformation will be useful for a LEO–LMO mission, for example.

The transformation is only valid when there is no desired plane change during the spiral (i.e., a planar-inclined orbit). The eccentricities and true anomalies of the initial orbits in two and three dimensions must be identical at the initial time but the transformation allows the initial inclination, right ascension, and argument of

periapsis to be different in the three-dimensional case compared with the two-dimensional solution. The acceleration magnitude and direction as well as the velocity with respect to the frame in the plane of the orbit must be the same as found for a two-dimensional spiral's acceleration history in the x–y plane. The frame in the plane of the orbit is defined by a unit vector in the radial direction, a unit vector along the angular momentum vector, and a third tangential unit vector in the plane of the orbit. The x values of the acceleration direction and velocity from the two-dimensional case must be along the radial unit vector of the orbital frame, whereas the y components of the acceleration and velocity lie along the tangential unit vector. The acceleration magnitude is the same in both the two- and three-dimensional solutions. The * terms in the rotation matrix are never used in the formulation.

$$\begin{bmatrix} e_x \\ e_y \\ e_z \end{bmatrix}_{3D} = \begin{bmatrix} A & B & * \\ C & D & * \\ E & F & * \end{bmatrix} \begin{bmatrix} e_r \\ e_T \\ e_h \end{bmatrix}_{\text{orbital}} \tag{37}$$

$$\begin{bmatrix} A \\ B \\ C \\ D \\ E \\ F \end{bmatrix} = \begin{bmatrix} \cos\Omega\cos\beta + \sin\Omega\cos i\sin\beta \\ \cos\Omega\sin\beta - \sin\Omega\cos i\cos\beta \\ \sin\Omega\cos\beta - \cos\Omega\cos i\sin\beta \\ \sin\Omega\sin\beta + \cos\Omega\cos i\cos\beta \\ -\sin i\sin\beta \\ \sin i\cos\beta \end{bmatrix} \tag{38}$$

$$\beta = -\omega - f \tag{39}$$

Using the transformation defined in Eq. (37) and the relationship between the acceleration unit direction vector and the velocity costates in Eq. (8) in the same way used to convert between the polar and Cartesian costates, the three-dimensional Cartesian velocity costates can be written in terms of the optimal values of the costates in two dimensions, appropriately placed in the orbital frame as discussed previously.

$$u_{\text{orbital}} = \begin{bmatrix} u_{x2D} \\ u_{y2D} \\ 0 \end{bmatrix} = \boldsymbol{\lambda}_v/\lambda_v \tag{40}$$

$$\begin{bmatrix} \lambda_{vx} \\ \lambda_{vy} \\ \lambda_{vz} \end{bmatrix}_{3D} = \begin{bmatrix} A\lambda_{vx2D} + B\lambda_{vy2D} \\ C\lambda_{vx2D} + D\lambda_{vy2D} \\ E\lambda_{vx2D} + F\lambda_{vy2D} \end{bmatrix} \tag{41}$$

The time derivative of Eq. (41) is taken and the appropriate terms from Cartesian costate equations of Eq. (13) are substituted to find the three-dimensional position costates.

$$\begin{bmatrix} \lambda_x \\ \lambda_y \\ \lambda_z \end{bmatrix}_{3D} = \begin{bmatrix} A\lambda_{x2D} + B\lambda_{y2D} \\ C\lambda_{x2D} + D\lambda_{y2D} \\ E\lambda_{x2D} + F\lambda_{y2D} \end{bmatrix} \tag{42}$$

Equations (41) and (42) transform the converged optimal costates found in the x–y plane for a two-dimensional spiral into the optimal costates in three dimensions in Cartesian coordinates where the initial orbit may have nonzero values for inclination, right ascension, and argument of periapsis and the same true anomaly and eccentricity as the initial two-dimensional orbit. The equivalent three-dimensional costates in spherical coordinates can be recovered by using the rotation defined in Eq. (1) to convert Eq. (37) into spherical coordinates. The derivation is not shown, but the process is then identical to the Cartesian case shown in Eqs. (37–42).

Optimal Escape Spirals with a Plane Change

For three-dimensional orbits, it is also desirable to target a specific inclination different from the initial orbit's inclination. Some work has focused on finding near-optimal orbital plane changes found from the optimal planar spiral found in two dimensions [17]. Other work finds optimal inclination changes during capture while also enforcing a final orbit shape [7], whereas the conditions presented next are for the optimal escape with a prescribed inclination change. A seventh unknown, ρ_{if}, and a seventh constraint are added to the boundary value problem presented in Eqs. (18) and (19). The Bolza function is updated to account for this new target.

$$G = \rho_{\varepsilon f}(\varepsilon_f - \varepsilon_{\text{tar}}) + \rho_{if}\left[\cos i_{\text{tar}} - v_\theta\cos\phi/\sqrt{\left(v_\theta^2 + v_\phi^2\right)}\right] \tag{43}$$

The mission presented is for a vehicle with initial mass of 100,000 kg and a power of 5 MW. First, the converged planar-inclined spiral was found by converting a converged set of costates in the two-dimensional case into the corresponding orbit in three dimensions. The orbit examined was a 20-day escape that was rotated to an inclination of 35 deg initially at the ascending node. The initial orbit is circular at 7500 km. This planar-inclined spiral at 35 deg was used as the first guess for a spiral where the final inclination at escape was desired to be 0 deg. Figures 5 and 6 show two views of the transfer, depicting the plane change, most of which takes place toward the end of the transfer at the farthest point from Earth.

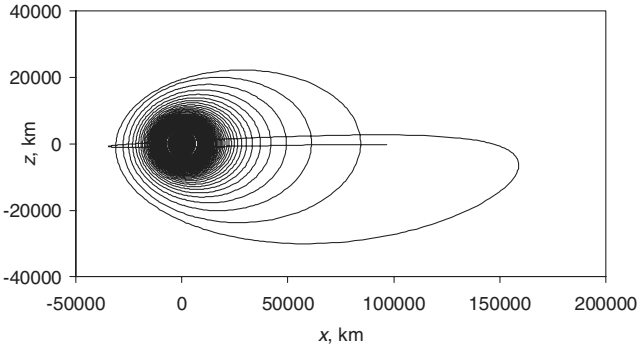

Fig. 5 Side view, 20-day spiral escape; $\Delta i = 35$ deg.

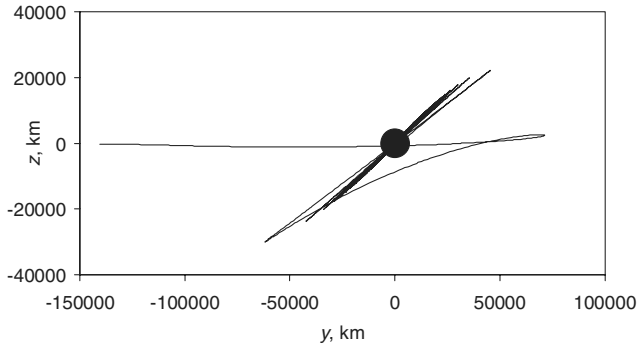

Fig. 6 Side view 2, 20-day spiral escape; $\Delta i = 35$ deg.

The control history is shown in Fig. 7, which shows the thrust and I_{sp}. Figure 8 shows the thrust direction, with alpha being the thrust angle from the radius vector in the r-θ plane, and beta is the out-of-plane angle above or below the r-θ plane.

Conclusion

Using the estimation techniques developed, long-duration, fuel-optimal escape/capture spirals can be easily determined with an indirect method. An adjoint control transformation is developed in spherical coordinates, allowing the user to make intelligent estimates of the costates. The behavior of the initial costates as the time of flight is increased is plotted and a power law curve fit is matched to the data. Using these curve fits, estimates for costates with longer times of flight are accurately extrapolated, forming an estimate of the costates that the numerical analysis easily converges. This process can be used for escape and capture spirals.

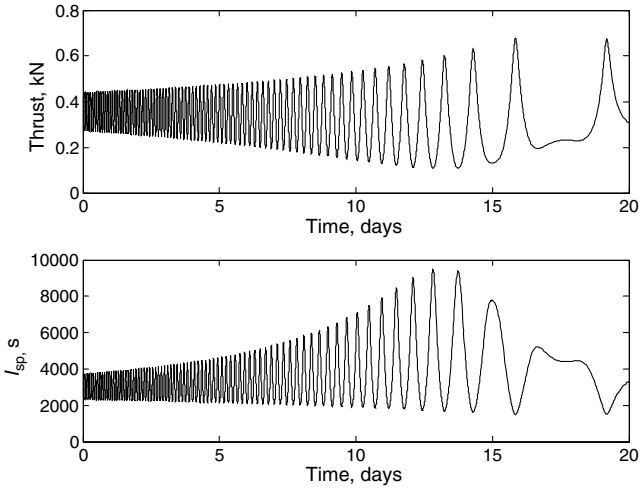

Fig. 7 Control history of 20-day spiral escape; $\Delta i = 35$ deg.

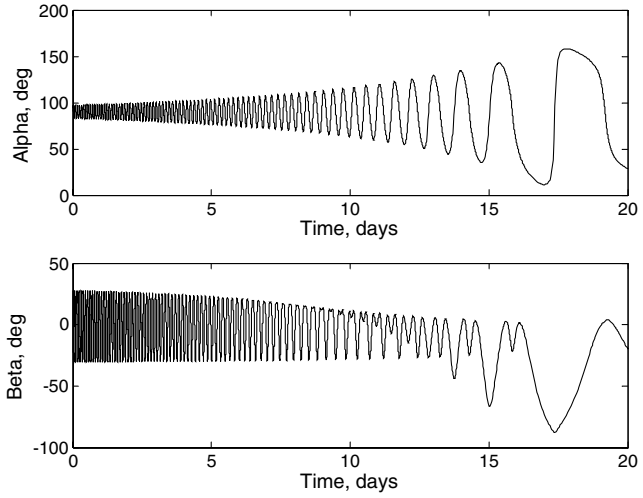

Fig. 8 Thrust angles of 20-day spiral escape, $\Delta i = 35$ deg.

Numerical verification of the algorithm presented was made by generating transformations that convert the two-dimensional polar costates into the corresponding Cartesian costates and vice versa. This also provided a means to analyze the behavior of the Cartesian costates, which are irregular when plotted vs the time of flight compared with their spherical equivalents. An additional set of transformations is derived that allows the two-dimensional Cartesian solution to be converted to three dimensions in either Cartesian or spherical coordinates as long as the semimajor axis, eccentricity, and true anomaly of both the two- and three-dimensional initial orbits are the same. These inclined planar solutions can be used as first guesses for three-dimensional spirals that have some required plane change.

A final transformation is developed that converts the costates from the general cost function, which is independent of initial mass and power, into the cost function that depends on the initial mass and power. This transformation is then used to find fuel-optimal spirals for a specific vehicle and additionally serves as the first guess for trajectories with I_{sp} or thrust constraints.

Acknowledgements

The authors would like to express thanks for the support and funding for this research provided in part by the National Defense Science and Engineering Graduate Fellowship, the Thrust 2000 UT Fellowship, and the NASA Johnson Space Center, AGN ISP Tools Grant, project no. NAG9-1476.

References

[1] Ranieri, C. L., and Ocampo, C. A., "Optimization of Roundtrip, Time-Constrained, Finite Burn Trajectories via an Indirect Method," *Journal of Guidance, Control, and Dynamics*, Vol. 28, No. 2, Mar.–Apr. 2005, pp. 306–314; also AAS Paper 03-572.

[2] Ranieri, C. L., and Ocampo, C. A., "Optimizing Finite-Burn, Round-Trip Trajectories with I_{sp} Constraints and Mass Discontinuities," *Journal of Guidance, Control, and Dynamics*, Vol. 28, No. 4, Jul.–Aug. 2005, pp. 775–781; also AAS Paper 04-231.

[3] Vadali, S. R., Nah, R., Braden, E., and Johnson, Jr. I. L., "Fuel-Optimal Planar Earth-Mars Trajectories Using Low-Thrust Exhaust Modulated Propulsion," *Journal of Guidance, Control, and Dynamics*, Vol. 23, No. 3, May–June 2000, pp. 476–482.

[4] Vadali, S. R., Nah, R., and Braden, E., "Fuel-Optimal, Low-Thrust, Three-Dimensional Earth-Mars Trajectories," *Journal of Guidance, Control, and Dynamics*, Vol. 26, No. 6, Nov.–Dec. 2001, pp. 1100–1107.

[5] Pierson, Bion L., and Kluever, Craig A., "Three-Stage Approach to Optimal Low-Thrust Earth-Moon Trajectories," *Journal of Guidance, Control, and Dynamics*, Vol. 17, No. 6, Nov.–Dec. 1994, pp. 1275–1282.

[6] Kluever, Craig A., and Pierson, Bion L., "Optimal Low-Thrust Three Dimensional Earth-Moon Trajectories," *Journal of Guidance, Control, and Dynamics*, Vol. 18, No. 4, July–Aug. 1995, pp. 830–837.

[7] Kluever, Craig A., and Pierson, Bion L., "Optimal Low-Thrust Earth-Moon Trajectories Using Nuclear Electric Propulsion," *Journal of Guidance, Control, and Dynamics*, Vol. 20, No. 2, Mar.–Apr. 1997, pp. 239–245.

[8] Guelman, M., "Earth-to-Moon Transfer with a Limited Power Engine," *Journal of Guidance, Control, and Dynamics*, Vol. 18, No. 5, Sep.–Oct. 1995, pp. 1133–1138.

[9] Thorne, James D., and Hall, Christopher D., "Approximate Initial Lagrange Costates for Continuous-Thrust Spacecraft," *Journal of Guidance, Control, and Dynamics*, Vol. 19, No. 2, Mar.–Apr. 1996, pp. 283–288.

[10] Thorne, James D., and Hall, Christopher D., "Minimum Time Continuous-Thrust Orbit Transfers," *Journal of the Astronautical Sciences*, Vol. 45, No. 4, Oct.–Dec. 1997, pp. 411–432.

[11] Ranieri, Christopher L., and Ocampo, Cesar A., "Indirect Optimization of Spiral Trajectories," American Astronautical Society Paper 05-372, 2005.

[12] Sauer, C. G., Jr., "Optimization of Multiple Target Electric Propulsion Trajectories," AIAA Paper 73-205, 1973.

[13] Hull, D. G., *Optimal Control Theory for Applications*, Springer, New York, 2003, pp. 276–316.

[14] Dixon, L. C. W., and Biggs, M. C., "The Advantages of Adjoint-Control Transformations When Determining Optimal Trajectories by Pontryagin's Maximum Principle," *Aeronautical Journal*, Vol. 76, Mar. 1972, pp. 169–174.

[15] Press, William H., *Numerical Recipes in FORTRAN 77: The Art of Scientific Computing*, Cambridge Univ. Press, New York, 1992, pp. 712–715.

[16] Anon., "NS11AD," Harwell Subroutine Library [online archives], http://www.cse.clrc.ac.uk/nag/hsl/ [cited 06 Dec. 2005].

[17] Schlingloff, H., "Control Laws for Optimal Spacecraft Navigation," *Journal of Spacecraft and Rockets*, Vol. 24, No. 1, 1987, pp. 48–51.